Deterministic, Nanoscale Fabrication of Mesoscale Objects

R. Mariella Jr., J. Gilmer, A. Rubenchik, M. Shirk

February 3, 2005

Disclaimer

Deterministic, Nanoscale Fabrication of Mesoscale Objects
Final Report for 3 years

Principal Investigator: Raymond Mariella Jr.
Responsible Directorate: Engineering
Primary Category of Work: Engineering and Manufacturing Processes
Secondary Category of Work: Materials Science and Technology
Type of Research: BASIC   Tracking Code: 02-ERD-014

Report Authors: R. Mariella Jr.; G. Gilmer; A. Rubenchik; M. Shirk

Summary

Project Description

Neither LLNL nor any other organization has the capability to perform deterministic fabrication of mm-sized objects with arbitrary, µm-sized, 3-D features and with 100-nm-scale accuracy and smoothness. This is particularly true for materials such as high explosives and low-density aerogels, as well as materials such as diamond and vanadium. The motivation for this project was to investigate the physics and chemistry that control the interactions of solid surfaces with laser beams and ion beams, with a view towards their applicability to the desired deterministic fabrication processes. As part of this LDRD project, one of our goals was to advance the state of the art for experimental work, but, in order to create ultimately a deterministic capability for such precision micromachining, another goal was to form a new modeling/simulation capability that could also extend the state of the art in this field. We have achieved both goals.

In this project, we have, for the first time, combined a 1-D hydrocode ("HYADES") with a 3-D molecular dynamics simulator ("MDCASK") in our modeling studies.

In FY02 and FY03, we investigated the ablation/surface-modification processes that occur on copper, gold, and nickel substrates with the use of sub-ps laser pulses. In FY04, we investigated laser ablation of carbon, including laser-enhanced chemical reaction on the carbon surface for both vitreous carbon and carbon aerogels. Both experimental and modeling results will be presented in the report that follows.

Results

The immediate impact of our investigation was a much better understanding of the chemical and physical processes that ensue when solid materials are exposed to femtosecond laser pulses. More broadly, we have better positioned LLNL to design a cluster tool for fabricating mesoscale objects utilizing laser pulses and ion-beams as well as more traditional machining/manufacturing techniques for applications such as components in NIF targets, remote sensors, including diagnostic systems, miniature fuels cells, and medical technologies.

Mission Relevance

This project supports the Laboratory's Stockpile Stewardship mission and aspects of the Homeland-Security mission.

Accomplishments and Results

In FY02 and early FY03, we combined the hydrodynamics and molecular-dynamics codes into a merged modeling/simulation capability (Rubenchik and Gilmer). This modeling team worked closely with the experimentalists (Shirk, Siekhaus, Baker) to study the interactions of fs laser pulses with copper, gold, and nickel substrates. One surprising result from the modeling was the observation of front-surface spallation, for laser pulses with fluence only slightly above the ablation threshold. We also demonstrated, both in experiments and in simulations, that the application of trains of the fs laser pulses, at sub-ablation fluences, could be used to smoothen μm-scale surface roughness in nickel substrates.

In FY04, using carbon substrates, we investigated the processes that occur with the use of laser pulses and oxygen ion beams to ablate the surface. With the laser, we studied the ablation process both in vacuum and also in air. Our main effort used vitreous carbon, both because it was readily available and because it was the easiest form of carbon to model. It was through our collaboration with colleagues at LBL (Siekhaus) that we studied the use of oxygen-ion beams to micromachine smooth features in vitreous carbon. We also studied laser ablation of carbon aerogels and were able to micromachine simple features into the surfaces of these aerogels.

Exit Plan

After the three years of research, we have moved LLNL's ability to contour difficult materials at the μm scale into a more deterministic framework. There are specialized applications for our new capability, such as micromachining of diamond, high explosives, or metals, such as vanadium, that do not machine well via single-point diamond turning, or ultra-low-density aerogels. However, within the rubric of msesoscale manufacturing, it is clear that there are two, more-important shortfalls that are in the "importance" queue, ahead of laser or ion-beam micromachining; namely:

non-destructive, 3-D characterization and

flexible, computer-assisted bonding/joining/assembly.

That notwithstanding, we can be sure that our new micromachining capabilities will be part of the Engineering vision for the future of computer-assisted design/computer-assisted mesoscale manufacturing.

Detailed Report

For modeling/simulation, we combined three-dimensional (3-D) molecular dynamics (MD) modeling code, MDCASK, with a 1-D hydrocode.

HYADES is a one-dimensional hydrocode with a wave equation solver that provides a good description of laser energy absorption, shock formation, and thermal transport, and is fast enough to follow system evolution for the hundreds of nanoseconds. The studies of material ablation by the short laser pulses consider the scales of materials modification and ejecta that are much smaller than the laser spot, thus a one-dimensional treatment of the problem is adequate. The code takes into account the change of the absorption during the pulse due to the change of electron density, spatial profile and temperature, as well as the transport of energy via the heated electrons.

In its present form, HYADES does not account for the resistance of the material to fracture, void nucleation in overheated liquids and other such effects that are crucial to the ablation of individual atoms and particles during laser irradiation and lack the capability to describe the system in 3 dimensions. MDCASK provides a full, 3-D atomic level description of the material, but does not include its interaction with the laser radiation. Also, because of its detailed nature, the MD calculation can treat only a small volume of material for a short time. We have successfully combined the two codes in such a way as to take advantages of the strengths of each approach, when modeling the interaction of sub-ps laser pulses with a solid surface. First we follow the laser-material interaction with HYADES. Then, well after laser pulse termination and the relaxation of the electron subsystem, the density, velocity, pressure and temperature profiles are passed on as initial conditions for the MD simulator. Initially, laser ablation was modeled using large-scale molecular dynamics (MD) simulations (via the parallel code MDCASK) of single-crystal copper. The computational cells contained from four to thirty million atoms. Interactions between the copper atoms were simulated using the embedded atom (EAM) potential of Mishin.

The description of thermal transport includes temperature-dependent thermal conduction and heat capacities. Thermal conduction is determined by the collision

frequency in the Drude model. The cold value of transport constants are matched with experimental data and interpolated to the hot plasma expression for an ideal plasma. The description takes into account the change of transport coefficients at melting point and pressure-induced shift of melting point according the Lindemann law. A rich diversity of phenomena was observed as a function of the pulse energy density, including the ejection of a liquid film. See Figure 1. Published observations of interference fringes that resulted from ablation using fs laser pulses are in excellent agreement with our simulations that show the ejection of a liquid layer. Three distinct regimes are exhibited: (i) a low energy regime with a minute ablation flux corresponding to evaporation of atoms from the hot copper surface; (ii) an intermediate regime where void nucleation and growth, or spall, causes the ejection of a stable liquid layer and particles, and (iii) high pulse energies where liquid droplets are ejected with a wide range of sizes. For 150-fs laser pulses on copper, this approach predicts void nucleation to occur within about 20 nm of the surface and, surprisingly, this void nucleation produces surface roughening, even below the ablation threshold.

Experimentally, our first studies with metal substrates included single-shot and multiple-shot ablation of single-crystal and polycrystalline, copper, gold, and nickel targets, using 150-fs laser pulses at 800-nm wavelength. For laser pulses only slightly above the threshold for ablation, results show that the residual surface roughness is relatively independent of the total depth of the ablation crater. See Figure 2. We also observed that initial surface scratches tended to be nucleation sites for the micropits that are formed during ablation. See Figure 3. Separate from this effect, linearly-polarized laser pulses generate interference effects that also create patterned surface ridges. Therefore, we studied how much influence pre-existing, sub-μm-spaced ridges, made by diamond turning of the surface prior to laser ablation could exert in controlling/limiting the surface ridges that typically result from the use of polarized light, when the two processes were set up to be perpendicular to each other. The results can be observed in Figures 4 and 5. In Figure 4, the orientation of the initial scratches and the laser polarization are parallel and the orientation of the resulting surface features follow the orientation of the scratches. In Figure 5, near the top of the micrograph, the initial-

condition, machined ridges did dominate the final surface features, but for the majority of the annulus that surrounds the central smoothly-ablated region, the influence of the polarization of the laser overwhelmed the initial conditions and the periodic, ridged, surface features that were created by the laser were perpendicular to the micromachined ridges.

The process of laser polishing was investigated as a way to reduce the amplitude of sub-µm surface perturbations caused by ablation, without affecting the longer-length-scale pattern formed by this process. Using a Monte-Carlo model of the crystal surface structure, we studied the effect of laser heating of the object to temperatures near the melting point. We found that it was effective, but that the time required was too great for efficient processing. However, by using laser pulses that produced a transient liquid layer of controlled thickness (surface melting), the time required to smoothen the surface could be reduced dramatically. Surface tension is the driving force that smoothens the surface, and the absence of anisotropies in transport in the liquid layer gave results that were superior to those from annealing below the melting point. The trade-off between the smoothening and freezing times determines the duration, period, and intensity of the polishing pulses. Results of using fs laser pulses to smoothen an artificially-roughened surface of nickel are shown in Figure 6. The surface had been roughened using single-point diamond micromachining, producing regular rows of µm-scale ridges. The laser processing smoothened these ridges, but did generate some nm-scale balls of nickel that decorate the surface.

For FY04, we investigated laser ablation of carbon, including chemically-assisted processes. We undertook this research, because the energy deposition that is required to perform direct sublimation of carbon is much higher than that to stimulate the reaction $2C + O_2 => 2\ CO$. Thus, extremely fragile carbon aerogels might survive the chemically-assisted process more readily than ablation via direct laser melting or sublimation. We had planned to start by studying vitreous carbon and move onto carbon aerogels. We were able to obtain flat, high-quality vitreous carbon, which was easy to work on, experimentally and relatively easy to model. We were provided with bulk samples of carbon aerogel by Dr. Joe Satcher, but the fabrication shop that would have prepared mounted samples for us was overwhelmed by programmatic assignments. We did study aligned carbon nanotubes, provided to us by colleagues at NASA Ames Research Center, as an alternative to aerogels. Dr. Gilmer started modeling the laser/thermally-accelerated reactions of carbon with H_2, rather than O_2, due to limited information on equation of state for CO.

In order utilize HYADES to model the interaction of fs laser pulses of 825-nm light with carbon, including vitreous carbon, we needed its dielectric function. Published experimental data were inadequate, therefore we undertook to measure the reflectivity of a sample of vitreous carbon with a mirror-like surface as a function of angle of incidence, for both S- and P-polarized laser pulses. Using the data that are plotted in Figure 13 and the Fresnel formulae for reflectivity, we calculated that the complex index of refraction for vitreous carbon is $n = 2.21 + 0.65i$.

We have extended our molecular dynamics models of ablation to include carbon in the form of graphite, vitreous carbon, and aerogels. The computer code has features that allow control of temperature, absorption of shock waves, and for the ejection of material from the computational cell. We form vitreous carbon atomic configurations by melting graphite in a microcanonical cell at a temperature of about 5000 K. Quenching the molten carbon at a controlled rate of cooling yields material with a structure close to that of the vitreous carbon produced in the laboratory. To represent the aerogel, we have a computer code that connects "graphite" rods to randomly placed points in the 3-D

computational cell. Ablation simulations yield results for vitreous carbon similar to our previous results with copper, usually involving the transient melting of the material above the threshold energy density. However, some fracturing in the solid regions occurs in this case, but was never observed in copper. These simulations are continuing, together with studies of the reaction of hydrogen with vitreous graphite at high temperatures. These reactions are qualitatively similar to that of oxygen with the carbon atoms at the surface, and the simulations should provide insight into the applicability of the use of chemical reactions to shape the surfaces of aerogels.
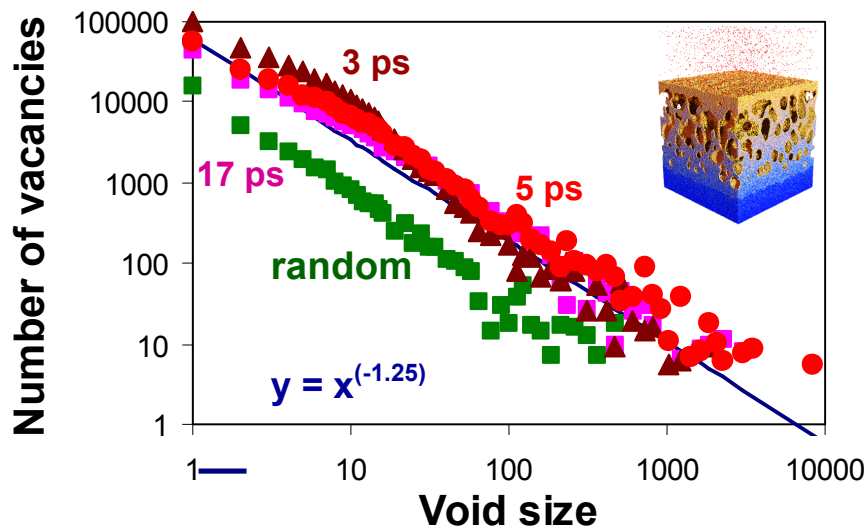
Voids nucleate during the initial phases of laser ablation and subsequently expand and coalesce, and this process releases most of the ablated material from the target. An understanding of surface roughening during ablation requires a detailed model of void formation and expansion. Our molecular dynamics models of materials such as carbon and of metals are ideal for such a study. This figure shows void sizes calculated by tracing connected vacant sites. Elapsed times after the laser pulse are indicated on the figure, and data for a random void distribution is shown. The similarity to the cluster size distribution in a random array of vacancies suggests that there is little or no barrier to void formation under ablation conditions, and this holds through much of the time period where the voids are coarsening.
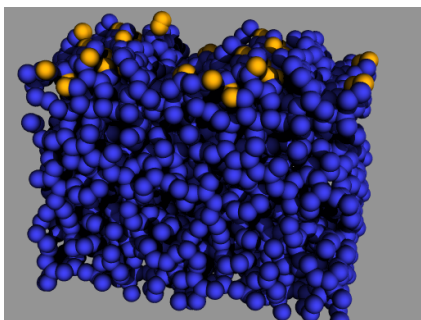
We are modeling the interaction of H with vitreous carbon using molecular dynamics potentials that have been developed for hydrocarbons. This figure shows a slab of vitreous carbon (blue spheres) interacting with hydrogen (yellow) at the top surface. These reactions are similar to those between oxygen and carbon, and provide insight for our experiments.

Since Dr. Siekhaus already used molecular-beam studies of a heated carbon surface reacting with a beam of O_2, we had an estimate of desired temperatures (2000 K) and expected reaction probabilities (max = 10%). Early modeling suggested a pronounced anisotropy in the strength of interaction of nm-diameter fibers with linearly-polarized light, and we have obtained samples of aligned carbon nanotubes from our collaborators at NASA in order to study this, experimentally.

We modeled the interaction of laser radiation with low-density aerosol. Due to the low density, the penetration depth is much longer then light wavelength. The aerogel can be modeled as a network of carbon strings (nanotubes) with diameter much smaller then the light wavelength. We demonstrated that the light absorption is sensitive to the mutual orientation of the carbon string and electric field. The absorption of light with electric field parallel to the string for 1-µm light is about 60 times higher than in the situation with electric field normal to the string. This effect greatly increases the ablation rate. Laser field penetrating in the aerogel explodes the points where electric field is parallel to the strings, breaking the string network and ejecting a lot of possibly-undamaged material. This is more efficient removal mechanism than traditional dense material evaporation and some experiments confirmed the enormously high aerogel ablation rate that was observed by Norris and co-workers (*J. Non-Cryst. Solids*, **281** (2001) pp 39-47).

When this project began, we had hoped to investigate the use of ion beams for surface micromachining. Dr. Siekhaus forged a collaboration with colleagues at LBL and the results of his efforts for vitreous carbon are illustrated in Figures 11 and 12. Note that even these very first experiments demonstrated that it was possible to micromachine very smooth features in the surface of vitreous carbon via oxygen ions.

Publications

Mesoscale Laser Processing using Excimer and Short-pulse Ti:Sapphire Lasers (M702)
M. D. Shirk, A. M. Rubenchik, G. H. Gilmer, B. C. Stuart, J. P. Armstrong, S. K. Oberhelman, S. L. Baker, A. J. Nikitin, R. P. Mariella Jr.
ICALEO® 2003, Oct. 13-16, 2003, Jacksonville, Florida USA
UCRL-JC-154591

"MEMS-based sensor systems", UCRL-CONF-204129, R. Mariella Jr., NNSA Futures Conference, Crystal City VA, May 2004

3rd International Conference: Computational Modeling and Simulation of Materials, Acireale, Sicily, Italy, May 30-June 4, 2004, *Short-Pulse Laser Ablation Simulated by Molecular Dynamics, Void Nulceation and Cluster Ejection,* G. H. Gilmer*, M. D. Shirk, A. M. Rubenchik, L. Zepeda-Ruiz, R. P. Mariella, T. Diaz de la Rubia, Invited Talk.

DOE-NSET Workshop on Artificially Structured Nanomaterials: Formation and Properties, Gatlinburg, TN, Oct. 13-15, 2003, *Thin Film Deposition and Manipulation of Surfaces using Laser Beams: Atomistic Modeling*, G. H. Gilmer, Invited Talk. UCRL UCRL-PRES-200845-DRAFT

WORKSHOP I: Fundamental Physical Issues in Nonequilibrium Interface Dynamics, Center for Scientific Computation and Mathematical Modeling, University of Maryland, Oct. 20-24, 2003,
*Laser Ablation and the Deposition of Metals: Large-Scale Molecular Dynamics Simulations***,** G. H. Gilmer, Invited Talk.

2nd International Workshop on Strength and Fracture, Berkeley Marina, California, January 7-9, 2004, *Short-pulse laser ablation of metals: Large-scale molecular dynamics simulations,* G.H. Gilmer, Invited Talk. UCRL-ABS-201337-DRAFT

American Physical Society March Meeting, Montreal, Canada, March 22-26, 2004, *Short-pulse laser ablation of metals: large-scale molecular dynamics simulations*. G. H. Gilmer, M. D. Shirk, A. M. Rubenchik, L. Zepeda-Ruiz, R. P. Mariella Jr, B. Sadigh, S. L. Baker, E. Bringa, Contributed Talk.

Materials Research Society Spring Meeting, San Francisco, CA, April 12-16, 2004, *Void Nulceation and Cluster Ejection during Short-Pulse Laser Ablation: Large- Scale Molecular Dynamics Simulations*, G. H. Gilmer, M. D. Shirk, A. M. Rubenchik, R. P. Mariella, L. Zepeda-Ruiz, S. L. Baker, B. Sadigh, Contributed Talk.

Directorate Review Committee, LLNL, May 2004, *Laser Shaping of Materials: Large- Scale Molecular Dynamics Simulations*, G. H. Gilmer, M. D. Shirk, A. M. Rubenchik, R.

P. Mariella Jr, A. M. Komashco, S. L. Baker, B. Sadigh, B. C. Stuart, M. A. Duchaineau, and T. Diaz de la Rubia; Poster. UCRL UCRL-POST-204026-DRAFT

The Third Annual Ann Arbor Symposium on Relativistic and Sub-Relativistic Intensity Lasers and their Applications, Ann Arbor, MI, June 2004, Ben Torralva & George Gilmer *Modeling the Damage Threshold*, Invited Talk

Record of Invention IL-11139
"Apparatus and Method of Micro-Polishing Materials"
Provisional Patent Filed, May 30, 2003

Manuscript submitted to Science
"Laser Ablation of Metals: Large-Scale Atomistic Simulations and Experiments"
G. H. Gilmer, M. D. Shirk, A. M. Rubenchik, R. P. Mariella, A. M. Komashko, S. L. Baker, B. Sadigh, M. A. Duchaineau, and T. Diaz de la Rubia; UCRL UCRL-JRNL-200163-DRAFT

Manuscripts in preparation
"Processing of dielectrics with ultrashort laser pulses", Rubenchik and Shirk

"Design and Implementation of a High-precision, Ultrashort Pulsed Laser Milling Machine", Shirk and Rubenchik

Figure Captions

Figure 1. Electron micrographs of copper substrates that have been ablated with 810-nm-wavelength, 150-fs laser pulses.

Figure 2. Representation of molecular-dynamics simulation of the early stages of the ablation process, showing nucleation and growth of voids below the surface ("cavitation"). The reddish band that moves downward is the progressing, compressive shock wave.

Figure 3. Electron micrographs of ablated copper surfaces, showing far more total material removal after 100 pulses than after 5 pulses, but with very similar surface features in the ablated areas.

Figure 4. Electron micrograph of a gold substrate, after laser ablation under similar conditions to that used in Figure 3b.

Figure 5. Electron micrographs of copper and gold substrates, showing the surface features that follow initial scratches in the surface. See arrows.

Figure 6. Graphical representation of molecular-dynamics simulation of laser ablation, showing the development and ejection of a thin, liquid layer ("spall").

Figure 7. Figures and information taken from Phys. Rev article that reported the observation of Newton's Rings, more consistent with the simulations shown in Figure 6 and less with their own Fig. 4.

Figure 8. Plots of atomic-force-microscopy characterization of diamond-turned nickel substrate.

Figure 9. Electron micrograph of the diamond-turned nickel substrate, after ablation with the fs laser. Note the reduced overall surface roughness, when compared with Figure 3, and note particularly the relative smoothness of the ablated region in the center, where the surface remained molten for the longest time.

Figure 10. Electron micrograph of diamond-turned nickel, after exposure to a fs-laser pulse that was close to the threshold for ablation. Note the relative smoothness and only a small number of nanoparticles remaining on the surface.

Pasted 3rd-year report

Figure Captions

Figure 1: SEM micrograph of vitreous carbon that has been micromachined to form a high-aspect-ratio pattern using a KrF excimer laser (248-nm wavelength pulses) via ablation trough a mask.

Figure 2: Optical profilometer image of vitreous carbon sample in Figure 1.

Figure 3: SEM micrographs of a 0.25-mm-wide"dimple" in carbon aerogel that has been micromachined via ablation with sub-ps laser pulses at 825 nm. Note that the process caused little collateral damage in the surrounding material.

Figure 4: SEM images of nano "hairs" and nanoparticles, formed collaterally, during high-power ablation of carbon aerogel using fs laser pulses at 825 nm and 1 KHz repetition rate.

Figure 5: Optical Profilometer image and line-out showing the uniformity that we were able to achieve in micromachining a trench, via oxygen-ion-beam ablation, in vitreous carbon. Conditions: 3 keV, 5-µA oxygen-ion beam, constant-speed, linear scan of substrate.

Figure 6: Optical Profilometer image and line-outs showing the uniformity that we were able to achieve in micromachining a "field of moguls", via oxygen-ion-beam ablation, in vitreous carbon. Conditions: 3 keV, 5-µA oxygen-ion beam, scan of substrate on a x-y stage moving with sinusoidally-modulated speed.

Fig.1 The combination of HYADES with MDCASK, modeling copper as the substrate, show that fs-laser pulses with fluence that only slightly exceeds the ablation threshold generate front-surface spall.
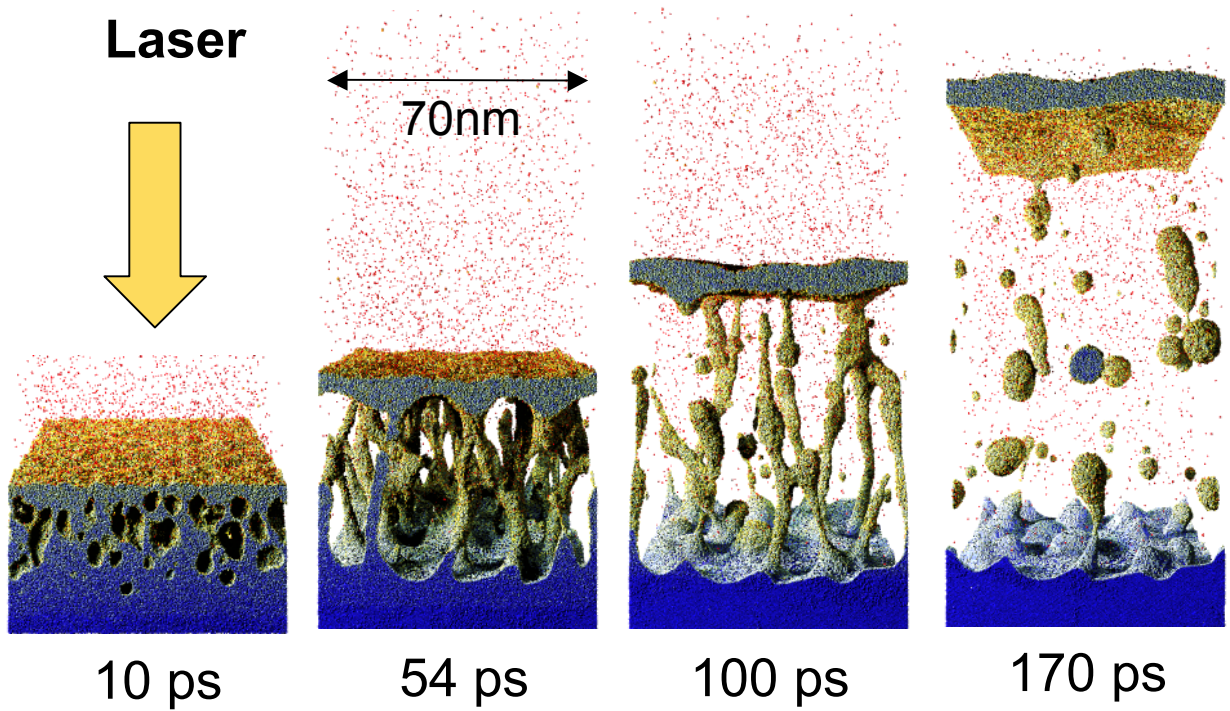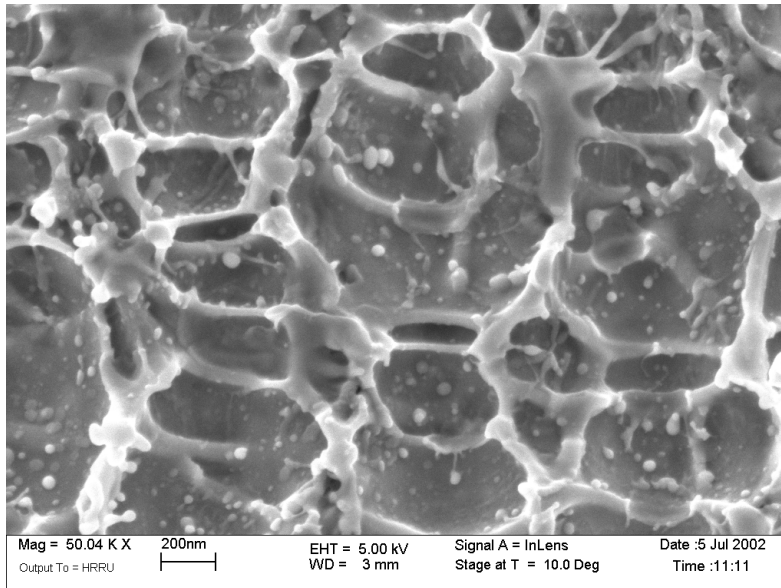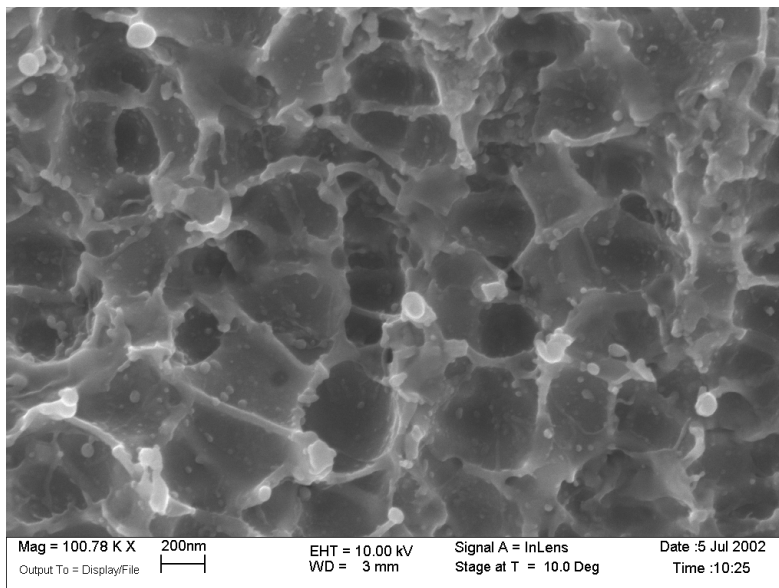

Laser

70nm

10 ps 54 ps 100 ps 170 ps

Fig.2 With copper as the substrate, further pulses and ablation do not significantly alter the residual surface features.

5 Pulses

100 Pulses

Fig.3 Again, with copper as the substrate, initial scratches nucleate instabilities with fs-laser ablation pulses. Black arrows indicate the location and orientation of scratches that were present in the surface, prior to exposure of the surface to the laser pulses.
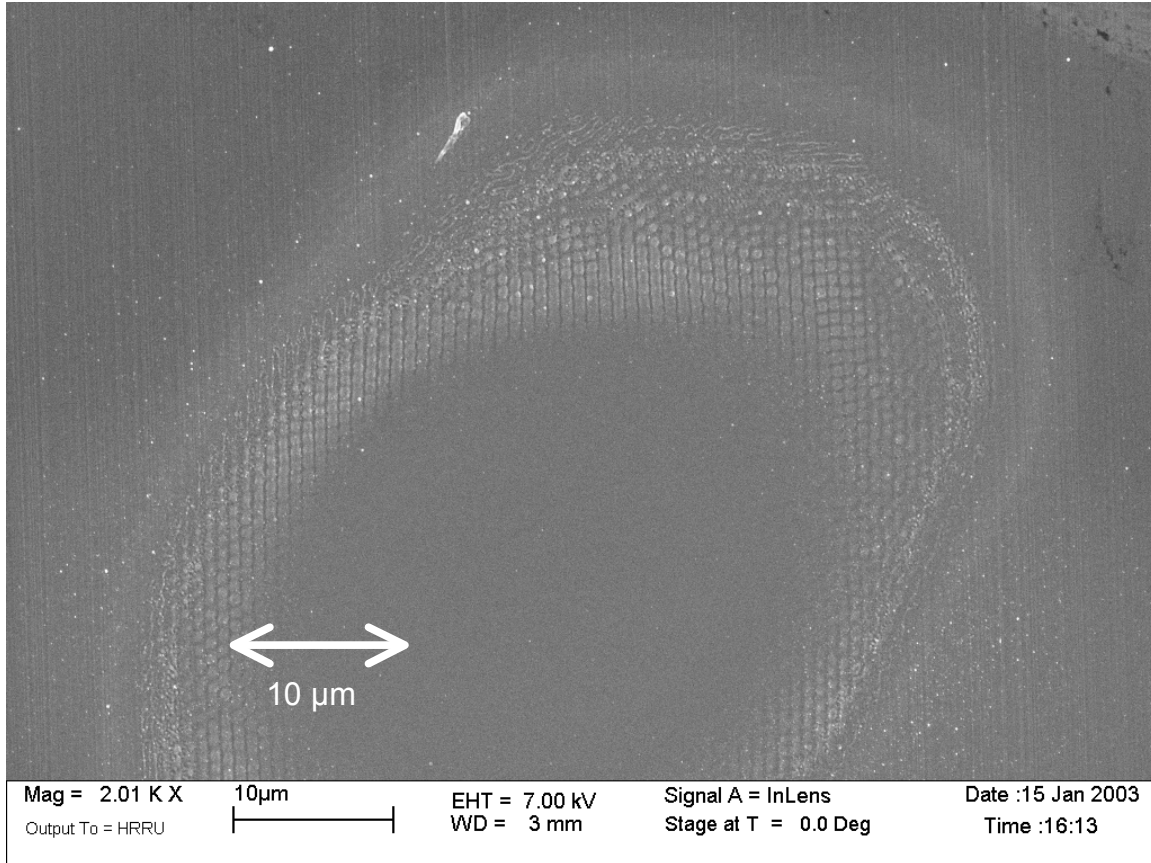

Copper
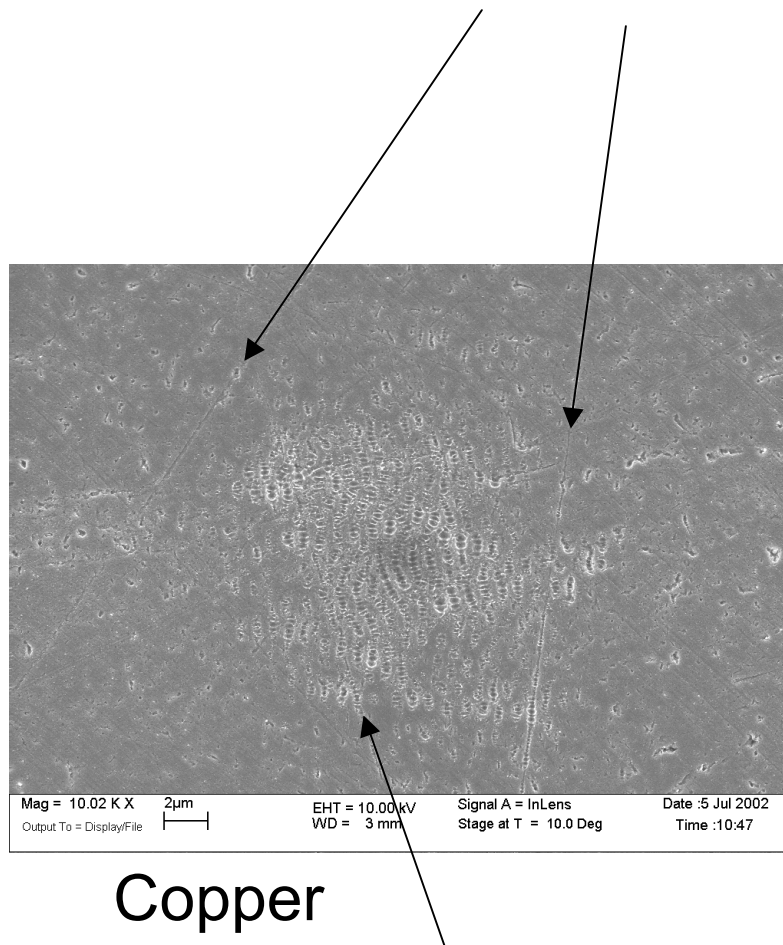
Fig.4 Fs-laser pulses, with fluence of 400 mJ/cm^2, removed 150 nm of material the center of the "dimple", and machined scratches in the nickel substrate nucleated regular rows of surface instabilities in an annulus around the dimple (Upper micrograph). As shown in the lower micrograph, at the center of the dimple, the surface displayed little roughness. (note scales).
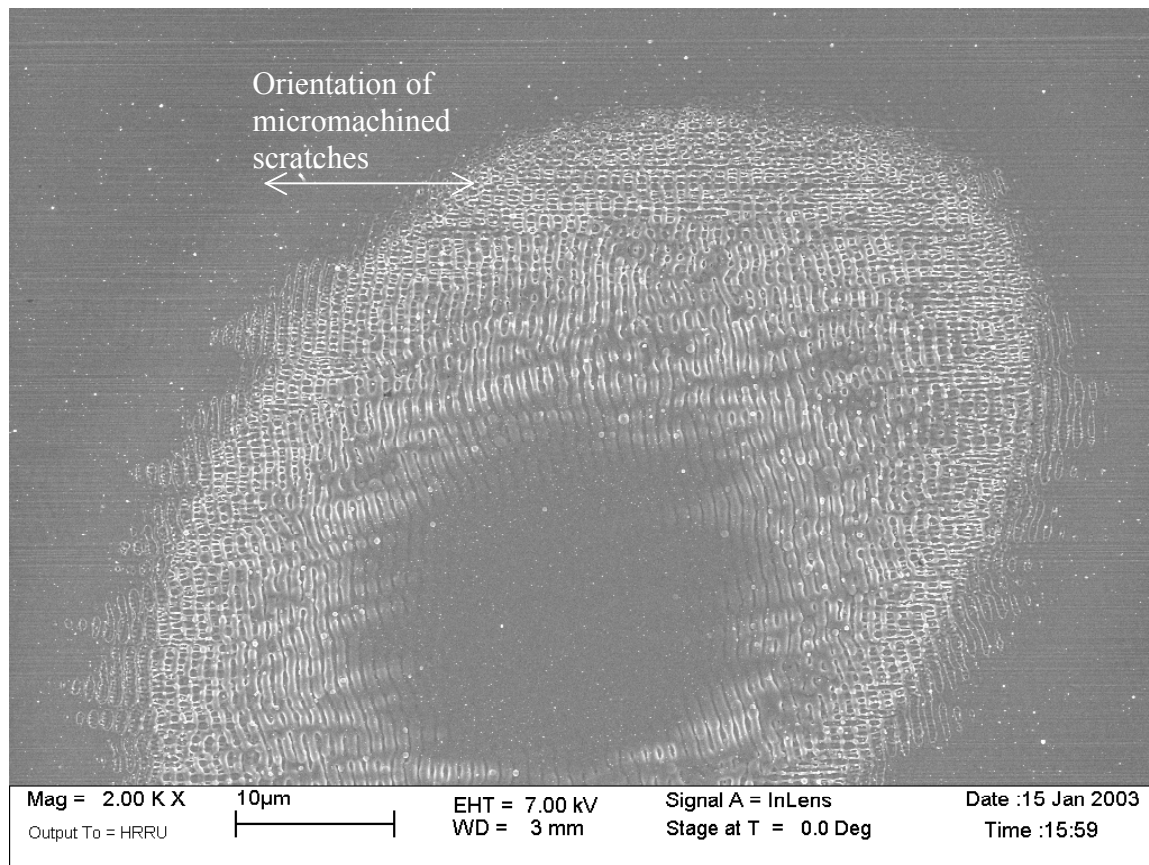

| Mag = 2.01 K X | 10µm | EHT = 7.00 kV | Signal A = InLens | Date :15 Jan 2003 |
| Output To = HRRU | | WD = 3 mm | Stage at T = 0.0 Deg | Time :16:13 |

Figure 5 – Nickel substrate, after fs laser pulses have ablated a dimple of 100-nm depth dimple. The laser was polarized perpendicular to the initial, micromachined scratches. In the upper portion of the dimple, the scratches are seen to nucleate regular rows of surface roughness (Also, see previous Figure.), but elsewhere in an annulus around the smooth center of the dimple, the effect of the laser polarization overwhelmed these initial surface conditions and generated larger-scale surface roughness with a regular pattern that followed the laser polarization.

200 nm

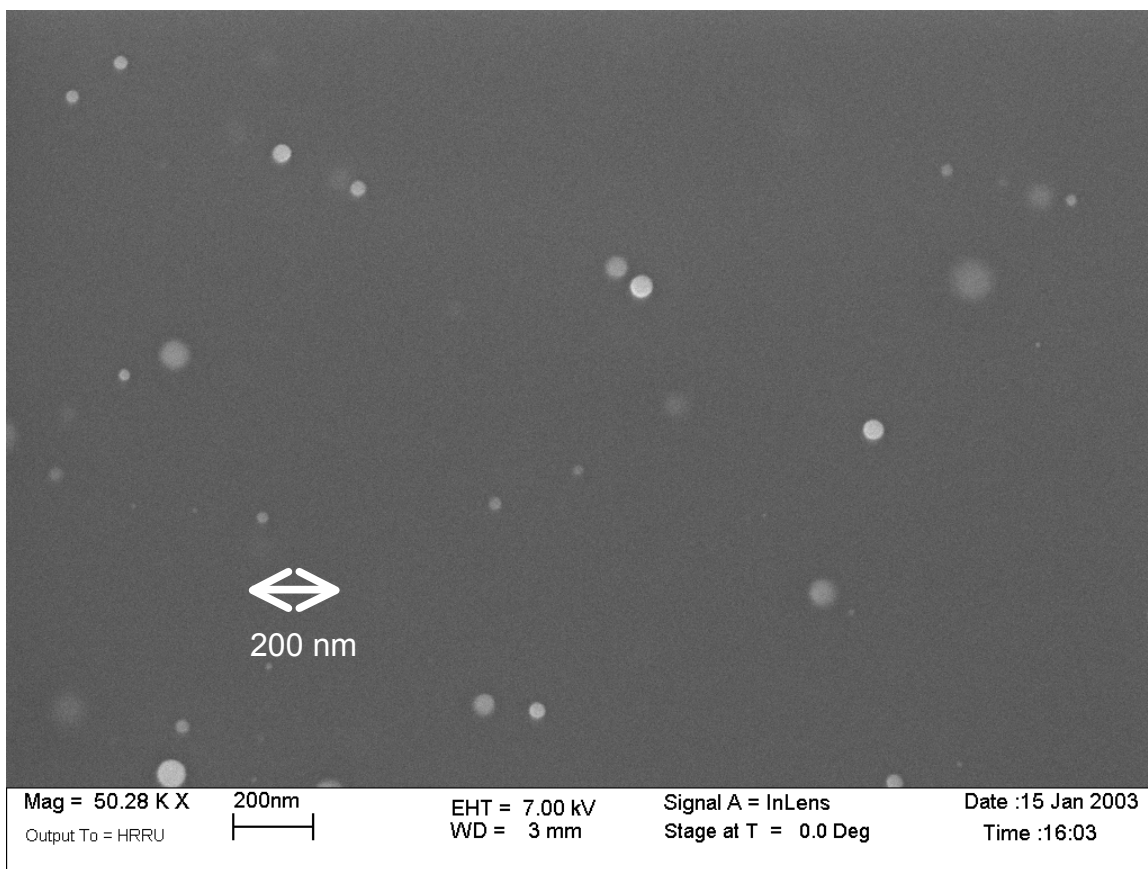| Mag = 50.28 K X | 200nm | EHT = 7.00 kV | Signal A = InLens | Date :15 Jan 2003 |
| Output To = HRRU | | WD = 3 mm | Stage at T = 0.0 Deg | Time :16:03 |

Figure 6. Micrograph of a nickel surface that originally had been covered with micromachined ridges. After smoothening via fs laser pulses, it shows a generally nanosmooth surface, except for a number of nm-scale balls of nickel that formed during the processing.
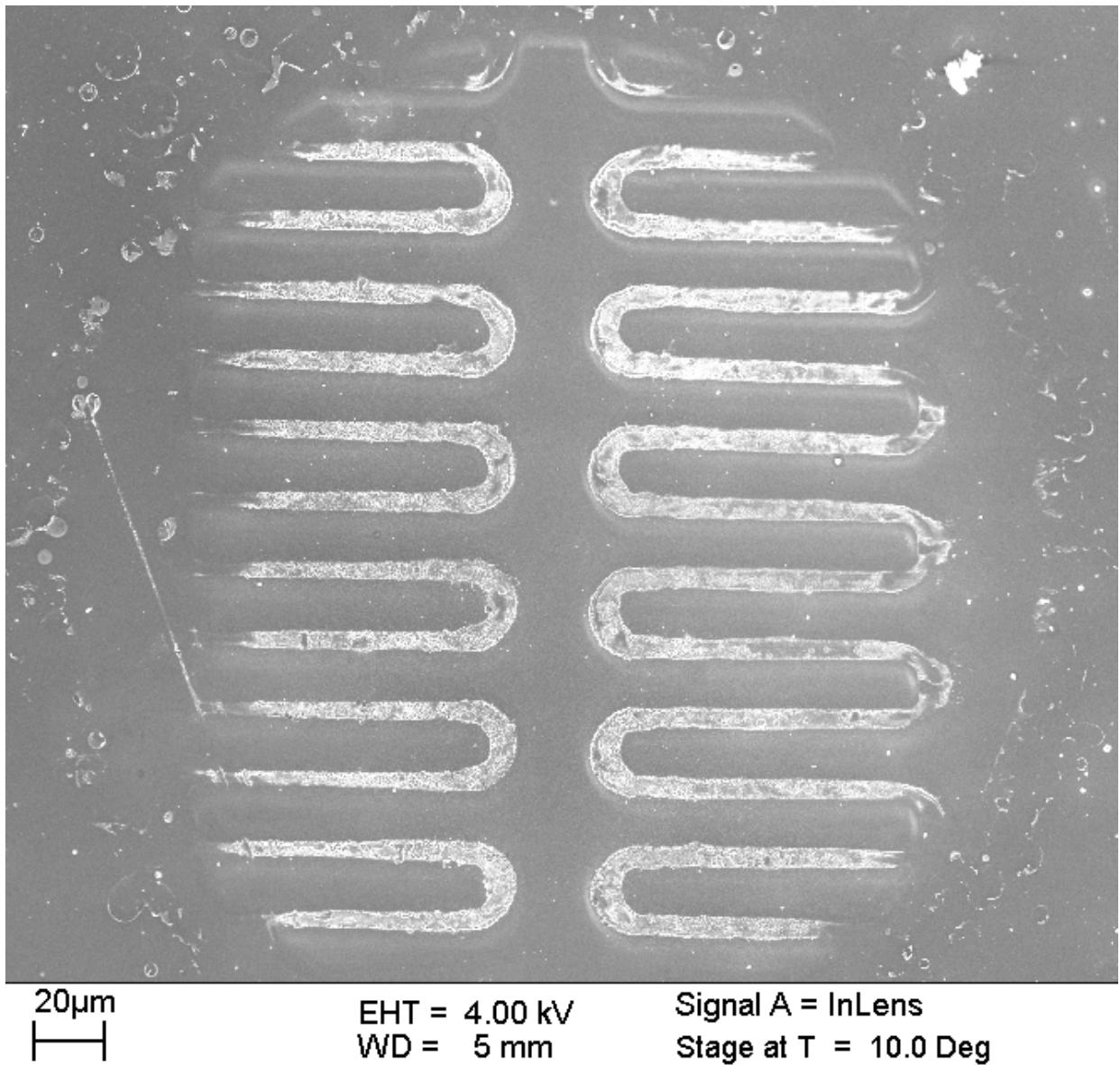
20μm

EHT = 4.00 kV
WD = 5 mm

Signal A = InLens
Stage at T = 10.0 Deg

Figure 7. Optical photograph of a surface feature that we micromachined into polyimide using ablation via 248-nm laser pulses from a KrF excimer laser. The pattern was created by passing the laser light through a "shadow mask" that was placed in the proximity of the surface.
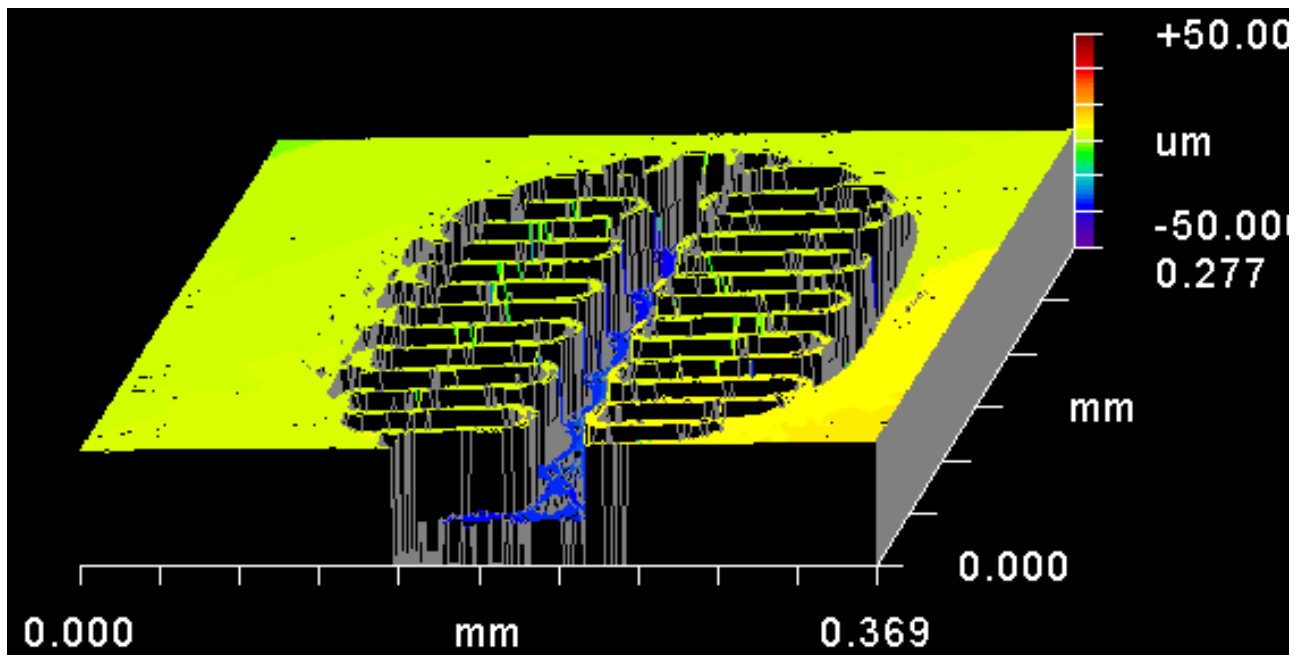
Figure 8a. Graphical, false-color image of the ablated surface from Figure 7, created using an optical profilometer. Note the steep vertical sidewalls of the features.

We measured the reflectivity for S- and P-polarized light on vitreous carbon using 100-fs light pulses at 800 nm. From this and the Fresnel model for reflection, we

Figure 8. Line out from optical profilometer along features shown in Figure 7.
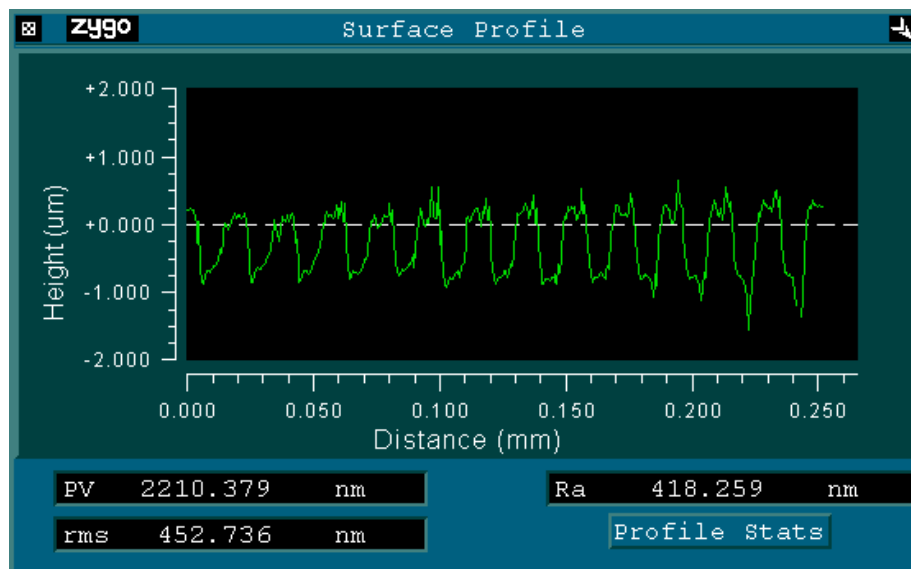
QuickTime™ and a
TIFF (Uncompressed) decompressor
are needed to see this picture.

Fig. 9. SEM micrographs of a 0.25-mm-wide"dimple" in carbon aerogel that has been micromachined via ablation with sub-ps laser pulses at 825 nm. Note that the process caused little collateral damage in the surrounding material.

Figure 10. Collateral effects on the surface of a carbon aerogel, following extensive ablative formation of a nearby trench.
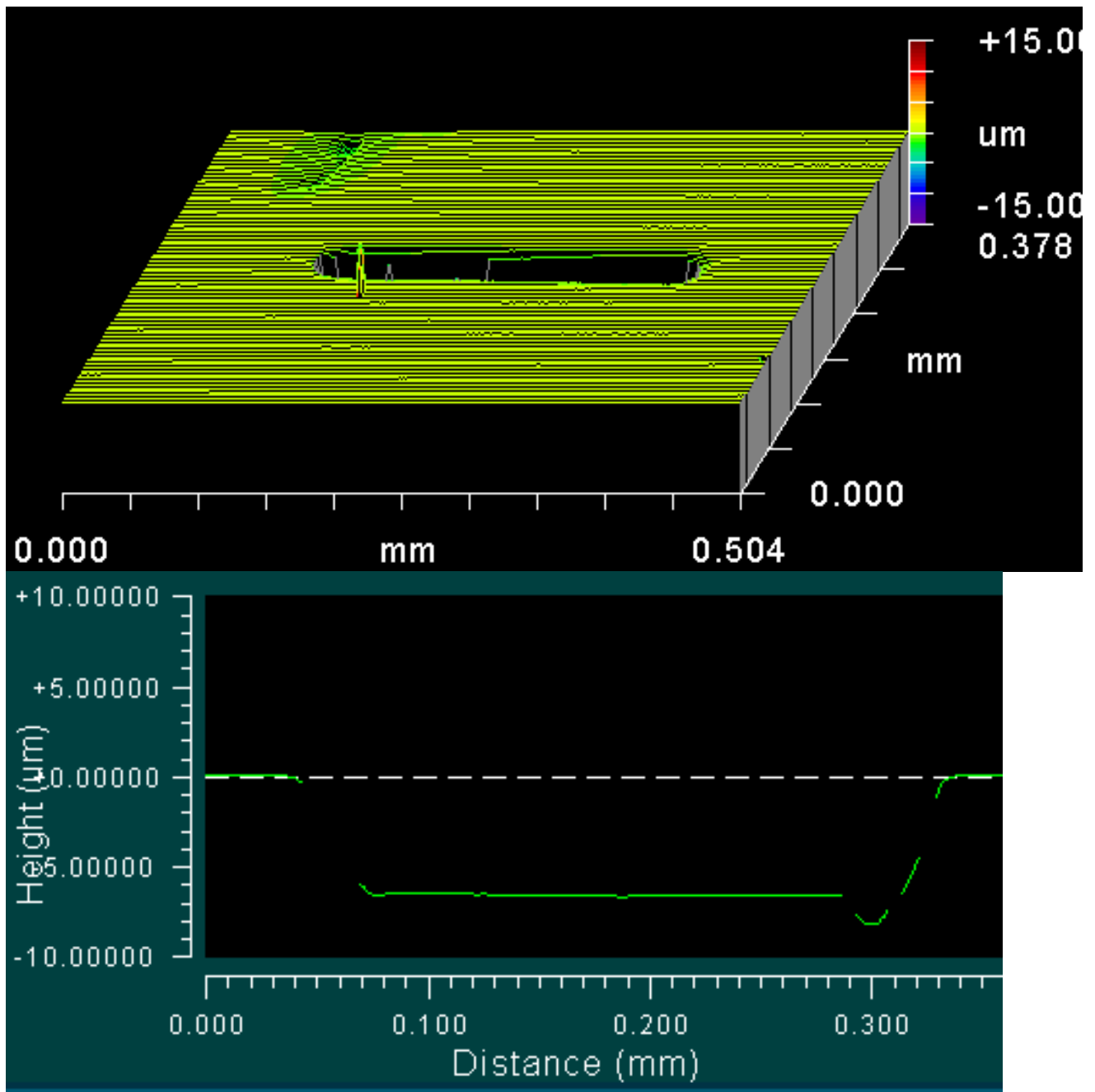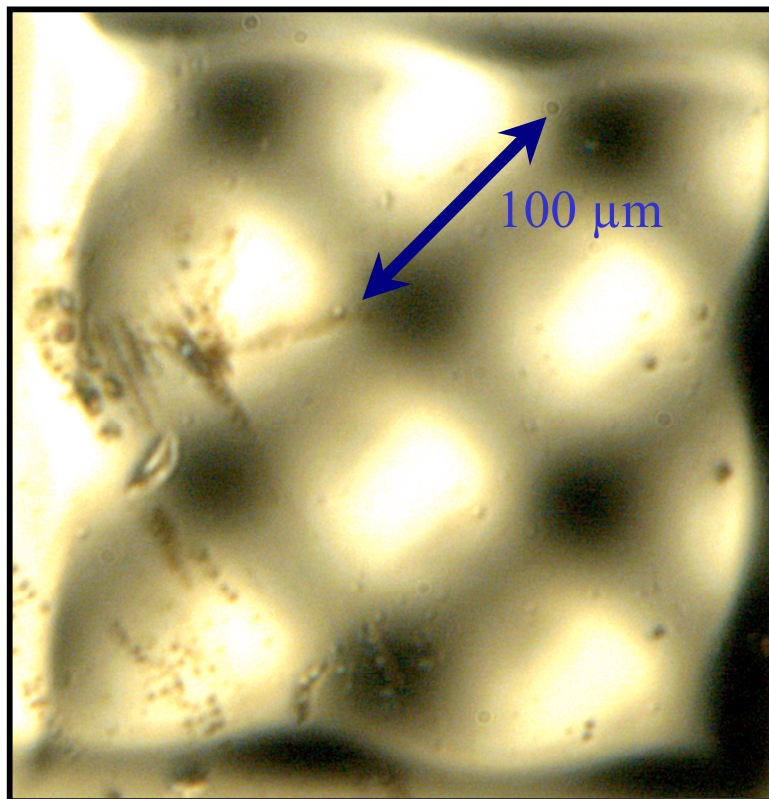
Fig 11. Optical Profilometer image and line-out showing the uniformity that we were able to achieve in micromachining a trench, via oxygen-ion-beam ablation, in vitreous carbon. Conditions: 3 keV, 5-µA oxygen-ion beam, constant-speed, linear scan of substrate.

Figure 12.

12a. Optical Profilometer image and line-outs showing the uniformity that we were able to achieve in micromachining a "field of moguls", via oxygen-ion-beam ablation, in vitreous carbon. Conditions: 3 keV, 5-µA oxygen-ion beam, scan of substrate on a x-y stage moving with sinusoidally-modulated speed.

100 µm

12b, 12c. Optical-profilometer image and line scans of sinusoidal moguls, micromachined in the carbon substrate. (see Figure 1a)
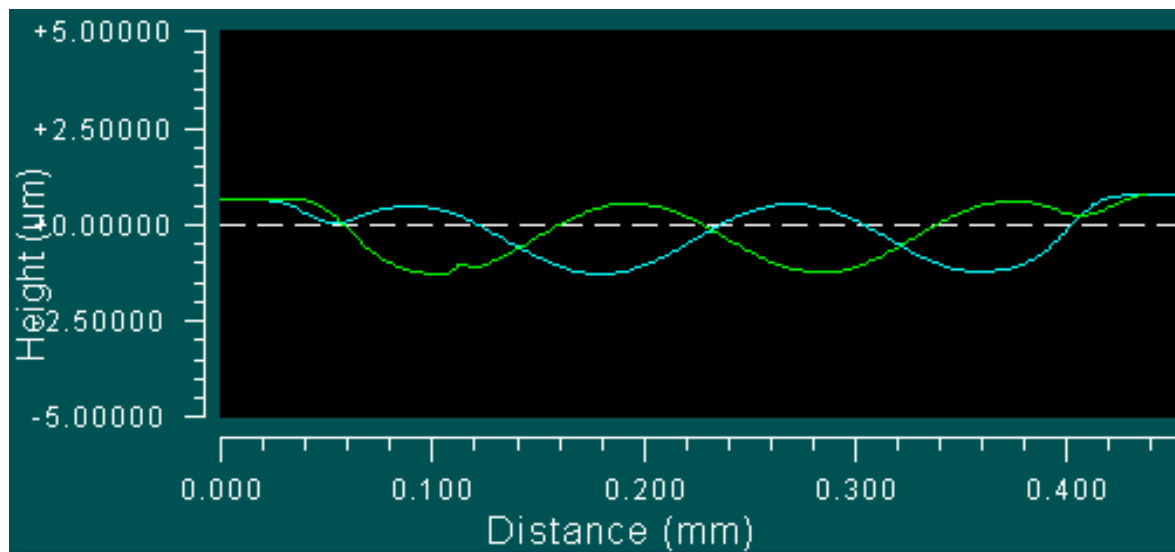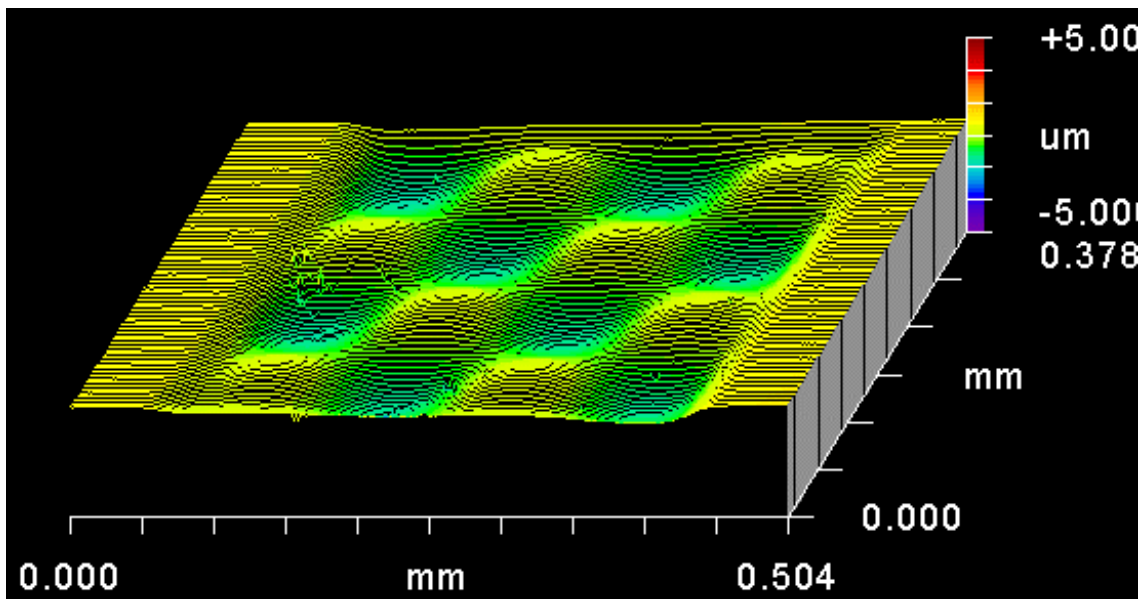
Fig. 13 Data plotted are our measurements of the reflectivity for S- and P-polarized light on vitreous carbon using 100-fs light pulses at 800 nm. From this and the Fresnel model for reflection, we calculated that n = 2.21 + 0.65i.

Fresnel Coeffs on vCarbon

Best fit with
n = 2.21, k = 0.65

Legend:
- Theory for P-pol
- Theory for S-pol
- Exp Data P-pol
- Exp Data S-pol

Incident Angle (°)